Mon. Not. R. Astron. Soc. **265,** 145–156 (1993)

The three-dimensional power spectrum measured from the APM Galaxy Survey – I. Use of the angular correlation function

C. M. Baugh and G. Efstathiou
Department of Physics, University of Oxford, Keble Road, Oxford OX1 3RH

Accepted 1993 May 11. Received 1993 March 30; in original form 1993 February 17

ABSTRACT

We describe a method of recovering the three-dimensional power spectrum of galaxy clustering from measurements of the angular correlation function $w(\theta)$. We apply the technique to $w(\theta)$ measured from the APM Galaxy Survey in the magnitude range $17 \leq b_J \leq 20$, using models for the redshift distribution of APM galaxies that reproduce the distributions measured in faint redshift surveys. The APM power spectrum is a power law at high wavenumbers, with slope $P(k) \propto k^{-1.25}$, as expected from the power-law slope of the angular correlation function. The power spectrum rises above the power law at wavenumbers $0.08\ h\ \mathrm{Mpc}^{-1} \lesssim k \lesssim 0.2\ h\ \mathrm{Mpc}^{-1}$. Systematic and random errors dominate the estimates of the power spectrum at wavenumbers smaller than $0.05\ h\ \mathrm{Mpc}^{-1}$. Our results are compatible with the power spectra measured from galaxy redshift surveys, but are more accurate. Our estimates of $P(k)$ for the APM survey are incompatible with the power spectrum of the standard $\Omega = 1$ cold dark matter (CDM) model, but can fit modified CDM models in the region $k \sim 0.1\ h\ \mathrm{Mpc}^{-1}$ (e.g. low-density CDM models, or mixed dark matter models). It remains to be seen whether these models can explain the APM power spectrum at higher wavenumbers, where the mass fluctuations are non-linear.

Key words: surveys – galaxies: clustering – dark matter – large-scale structure of Universe.

1 INTRODUCTION

The angular correlation function measured from the APM Galaxy Survey (Maddox et al. 1990a, hereafter M90) provides strong evidence for large-scale structure in the galaxy distribution on scales $\gtrsim 10\ h^{-1}$ Mpc.[1] Recent analyses of galaxy redshift surveys, e.g. the QDOT (Efstathiou et al. 1990a; Saunders et al. 1991) and 1.2-Jy (Fisher et al. 1993) surveys of *IRAS* galaxies, the CfA (Vogeley et al. 1992) and Stromlo/APM (Loveday et al. 1992b) redshift surveys, also provide evidence for large-scale power in the galaxy distribution, but the results on scales $\gtrsim 10\ h^{-1}$ Mpc are noisy, because the samples are small. In addition, the power spectra measured from redshift surveys are affected by distortions between real-space and redshift-space caused by peculiar velocity fields (see Kaiser 1987). It is therefore interesting to investigate whether the three-dimensional power spectrum of the galaxy distribution in real space can be recovered from the angular statistics measured from the APM survey. The APM survey samples a much larger volume of space ($\sim 10^8\ h^{-3}$ Mpc^3) than any redshift survey yet available, though a knowledge of the redshift distribution of the APM galaxies is required to recover three-dimensional statistics.

At first sight our approach might seem unduly elaborate. After all, it is possible to test models by projecting theoretical power spectra, $P(k)$, or spatial correlation functions, and comparing with the angular correlation function, $w(\theta)$, measured from the survey. This is the approach that we and others have adopted in the past (e.g. M90; Efstathiou, Sutherland & Maddox 1990b). Alternatively, one can pick a parametric form for the power spectrum and adjust the parameters until one gains a satisfactory fit to $w(\theta)$ (e.g. Peacock 1991). However, as we demonstrate in Section 4, a numerical inversion of $w(\theta)$ can reveal features and bumps in the power spectrum which would be difficult to parametrize in a simple way, and hence might escape detection unless one had some prior expectation of their presence. The numerical inversions also show clearly how the shape of the power spectrum is affected by random and systematic errors in the data.

[1]Throughout this paper h denotes Hubble's constant H_0 in units of $100\ \mathrm{km\ s^{-1}\ Mpc^{-1}}$.

Fall & Tremaine (1977) and Parry (1977) discuss an inversion, using Mellin transforms, of Limber's (1954) equation which relates the spatial two-point galaxy correlation function $\xi(r)$ to the angular correlation function $w(\theta)$. However, Mellin transforms are extremely cumbersome, and this technique would be difficult to apply to realistic models of the redshift distribution of a galaxy survey. Instead we use Lucy's (1974) algorithm, which we show leads to stable inversions, can be applied to kernels with a complex form, and can be used to recover the three-dimensional power spectrum directly from $w(\theta)$. We describe the inversion for the power spectrum in two dimensions in a subsequent paper, Baugh & Efstathiou (1993).

The layout of this paper is as follows. In Section 2, we derive the integral equation relating the three-dimensional power spectrum to the angular correlation function. A model for the redshift distribution of galaxies in the APM survey is presented in Section 3. Section 4 describes the numerical inversion of the integral equation using Lucy's method, and we present tests using power spectra of known functional form. This machinery is applied to the APM Galaxy Survey in Section 5, and the results are discussed in Section 6.

2 THE INTEGRAL EQUATION

The spatial two-point galaxy correlation function $\xi(r, t)$ is related to the angular correlation function $\omega(\theta)$ by Limber's equation. If we assume that clustering is independent of luminosity, and that the correlation function is negligible on scales comparable to the depth of the survey, Limber's equation can be written as

$$w(\varpi)=\frac{2\int_0^\infty\int_0^\infty x^4F^{-2}a^6p^2(x)\xi(r,t)\,\mathrm{d}x\,\mathrm{d}u}{[\int_0^\infty x^2F^{-1}a^3p(x)\,\mathrm{d}x]^2} \tag{1a}$$

(Peebles 1980, §50.16). The selection function, $p(x)$, is the probability that a galaxy at coordinate distance x is detected in the survey, and the metric is

$$\mathrm{d}s^2=c^2\,\mathrm{d}t^2-a^2[\mathrm{d}x^2/F^2(x)+x^2\,\mathrm{d}\theta^2+x^2\sin^2\theta\,\mathrm{d}\phi^2], \tag{1b}$$

where $F(x)$ depends on the cosmological model (see equation 6 below). The physical separation between galaxy pairs, separated by an angle θ on the sky, is

$$r^2=a^2[u^2/F(x)^2+x^2\varpi^2]^{1/2}, \tag{1c}$$

$$\varpi=2\sin(\theta/2), \tag{1d}$$

for separations that are small in comparison to the depth of the sample. We use the variable ϖ (equation 1d) rather than θ, so that the angular correlation function is defined over the finite range $0\le\varpi\le2$; this sets an upper limit to the angular variable as required for the inversion described in Section 4. The relativistic version of Limber's equation has been derived by Groth & Peebles (1977) and Phillips et al. (1978).

The surface density of galaxies in the survey is

$$\mathcal{N}=\int_0^\infty\frac{x^2}{F(x)}a^3p(x)\,\mathrm{d}x=\frac{1}{\Omega_s}\int_0^\infty\frac{\mathrm{d}N}{\mathrm{d}z}\,\mathrm{d}z, \tag{2}$$

where $(\mathrm{d}N/\mathrm{d}z)\,\mathrm{d}z$ is the number of galaxies in the redshift range z to $z+\mathrm{d}z$ in a survey of solid angle Ω_s. Thus, rather than making a model for the selection function based on the galaxy luminosity function, its evolution, k-corrections etc. (see M90), $p(x)$ can be expressed in terms of the redshift distribution $(\mathrm{d}N/\mathrm{d}z)$. This is the approach adopted in this paper, and it is described in Section 3 (see also Efstathiou et al. 1991).

The two-point correlation function is related to the three-dimensional power spectrum $P(k, t)$ by

$$\xi(r,t)=\frac{1}{2\pi^2}\int_0^\infty P(k,t)\frac{\sin(kr/a)}{(kr/a)}k^2\,\mathrm{d}k, \tag{3}$$

and k is a comoving wavenumber. If we parametrize the evolution of $P(k, t)$ as

$$P(k,t)=\frac{P(k)}{[1+z(t)]^\alpha}, \tag{4}$$

then, from (1a),

$$w(\varpi)=\int_0^\infty P(k)\,kg(k\varpi)\,\mathrm{d}k. \tag{5a}$$

Hence the integral equation takes a particularly simple form, where the kernel $g(k\varpi)$ is given by

$$g(k\varpi)=\frac{1}{2\pi}\frac{1}{(\mathcal{N}\Omega_s)^2}\int_0^\infty\frac{F(x)}{(1+z)^\alpha}\left(\frac{\mathrm{d}N}{\mathrm{d}z}\right)^2\left(\frac{\mathrm{d}z}{\mathrm{d}x}\right)J_0(k\varpi z)\,\mathrm{d}z, \tag{5b}$$

where

$$x=\frac{2c}{H_0}\left(1-\frac{1}{\sqrt{1+z}}\right),\qquad F(x)=1\qquad(\Omega_0=1), \tag{6a}$$

$$x=\frac{cz}{H_0(1+z)}\left(1+\frac{z}{2}\right),\qquad F(x)=\left[1+\left(\frac{H_0x}{c}\right)^2\right]^{1/2}$$

$$(\Omega_0=0). \tag{6b}$$

General expressions for x and $F(x)$ for other values of Ω_0 are given by Peebles (1980, §50.16). The non-relativistic version of (5) has been derived independently by Peacock (1991).

The assumption that $P(k, t)$ is a separable function of k and t (equation 4) is clearly an oversimplification. However, as it is impossible to invert a general function of two variables from an observed function of one variable, some simplifying assumption is required to model the evolution of $P(k, t)$. Fortunately, the median redshift range of $b_J\sim20$ APM galaxies is relatively low ($z_m\sim0.2$, see Section 3), and so the correction for the evolution in $P(k)$ is small. We therefore adopt the simple model of equation (4), and show how the results change as we vary the parameter α. Also, since the median redshift in the APM Survey is low, our results are relatively insensitive to the cosmological model, and we demonstrate this by using the redshift–distance relations for the $\Omega_0=1$ and $\Omega_0=0$ models given in equations (6).

3 THE REDSHIFT DISTRIBUTIONS AND THE FORM OF THE KERNEL

To evaluate the kernel (5b), we need a model for the redshift distribution of galaxies in the APM survey. We therefore investigated the redshift distribution of the deep pencil beam surveys of Broadhurst, Ellis & Shanks (1988) and Colless et

al. (1990, 1993). In these surveys, redshifts have been measured for galaxies in the magnitude range $20 \le b_J \lesssim 22.5$ in several small fields. If the solid angle of the ith field is Ω^i, the sampling rate f_s^i, and the redshift completeness f_c^i, we define a weight w^i for each galaxy in field i as

$$w^i = \frac{\Omega_i f_s^i f_c^i}{\Omega_*},$$

where Ω_* is a standard solid angle which we set to one square degree. We compute the mean weighted count of galaxies per square degree in redshift bins of width $\Delta z = 0.05$ averaged over all fields which overlap a specified magnitude range. This results in redshift histograms that use all of the redshift data in the surveys.

We have parametrized the redshift distribution as a function of apparent magnitude $m \equiv b_J$ by the formula

$$dN = A(m) z^2 \exp\left[-\left(\frac{z}{z_c(m)}\right)^{3/2}\right] dz, \qquad (7)$$

where the median redshift is given by

$$z_m = 1.412 z_c, \qquad (8a)$$

$$z_m(m) = 0.016(b_J - 17)^{1.5} + 0.046, \qquad b_J \ge 17. \qquad (8b)$$

The coefficient $A(m)$ is determined by the surface density of galaxies,

$$A(m) = \frac{3\mathcal{N}(m)\Omega_s}{2 z_c(m)^3}, \qquad (9a)$$

and we approximate $\mathcal{N}$ by a power law,

$$\mathcal{N}(m) = \frac{B 10^{0.45m}}{\Omega_s} \qquad (9b)$$

(see Maddox et al. 1990c). A more accurate parametric form for $A(m)$ is not required, since the normalization of the distribution (7) affects the shape of the redshift distributions predicted only for surveys in which galaxies are selected in magnitude slices. For our application, we use a wide magnitude slice, $17 \le b_J \le 20$, and so the lower magnitude limit is unimportant.

The specific functional form of equation (7) was chosen to provide an acceptable match to the deep redshift histograms (see Fig. 1), whilst simultaneously fitting models of the redshift distribution for catalogues limited at bright magnitudes ($b_J \sim 17$–18), for which we used redshift distributions computed from the luminosity function derived from the Stromlo/APM redshift survey (Loveday et al. 1992a). Equations (7) and (8) thus provide an accurate description of the redshift distributions over the entire magnitude range of the APM Galaxy Survey ($17 \lesssim b_J \lesssim 20.5$), though in this paper we are interested in the distributions of samples limited towards the faint end of this range. These models are discussed in further detail by Maddox et al. (in preparation). The median redshift (8) predicted by this model matches reasonably well even the medians of the faintest redshift surveys (Cowie, Songaila & Hu 1991) which indicate $z_m \sim 0.4$ at $b_J \sim 24$. The effects of errors in the redshift distribution on the inverse of $w(\theta)$ are discussed in Section 5.

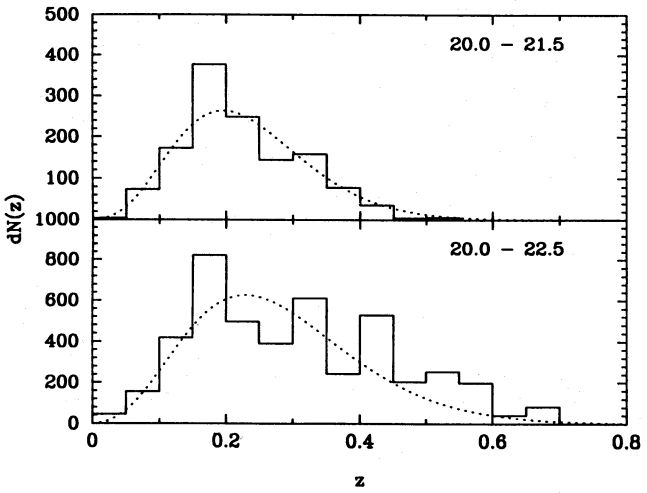

Figure 1. Redshift distributions (normalized as described in the text) for galaxies in the magnitude ranges 20–21.5 and 20–22.5. The data are from the deep redshift surveys of Broadhurst et al. (1988) and Colless et al. (1990, 1993). The dotted lines show the redshift distributions calculated from the model of equations (7)–(9).

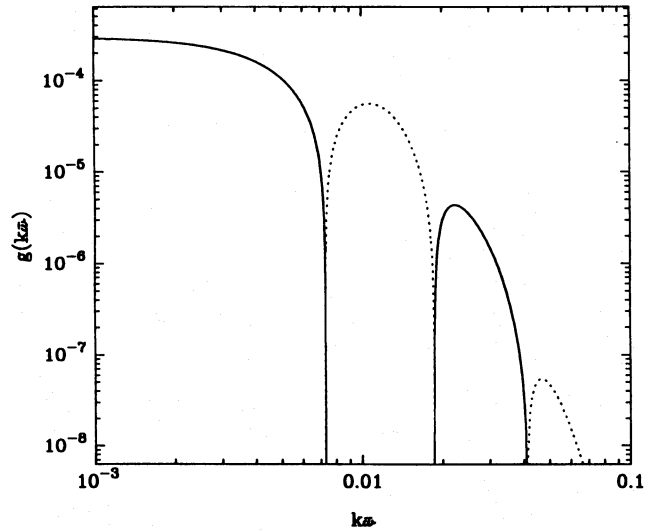

Figure 2. The kernel $g(k\varpi)$ for APM galaxies in the magnitude range $17 \le b_J \le 20$. We have assumed $\alpha = 0$ and a spatially flat background cosmology with $\Omega = 1$. The dotted portions of the curve show regions where $g(k\varpi)$ is negative. The abscissa is in units of h Mpc^{-1}.

Fig. 2 shows a plot of the kernel $g(k\varpi)$ for the magnitude slice $17 \le b_J \le 20$, assuming $\alpha = 0$ and $\Omega = 1$. Notice that it has three zero crossings over the range of $k\varpi$ shown. The first zero crossing defines a characteristic value of the argument $(k\varpi)_{crit}^{-1} \sim 150\ h^{-1}$ Mpc; angular correlations on scales ϖ are sensitive mainly to wavenumbers $k \lesssim (150\varpi\ h^{-1}\ \mathrm{Mpc})^{-1}$. For shallower catalogues, $(k\varpi)_{crit}^{-1}$ shifts to larger values.

4 NUMERICAL INVERSION OF THE INTEGRAL EQUATION

4.1 Inversion by Lucy's method

We invert equation (5) using Lucy's iterative method (Lucy 1974). We replace the integral in (5a) by a sum over N equally spaced intervals in $\ln k$ (typically 30 intervals over the range $3\times10^{-3}\lesssim k\lesssim 30$ h Mpc^{-1}). Thus for the rth iteration

$$w^r(\varpi_j)=\sum_i P_i^r k_i^2 g(k_i\varpi_j)\Delta \ln k. \tag{10}$$

We supply an initial guess for $P_i k_i^2$ (usually a power law), and compute w^r from equation (10). This is followed by a new estimate of the power spectrum:

$$\tilde{P}_i^{r+1}=P_i^r\frac{\sum_j[w^o(\varpi_j)/w^r(\varpi_j)]\,g(ki\varpi_j)}{\sum_j g(k_i\varpi_j)}, \tag{11a}$$

where $w^o(\varpi)$ is the observed angular correlation function, and the sums extend over typically 60 logarithmically spaced bins in the variable ϖ. Applying equations (10) and (11) to the tests described below, we sometimes found that the iterations did not converge smoothly to a solution. The stability of the algorithm was improved by smoothing the revised estimate of $\tilde{P}_i^{r+1}$, and by limiting the change in P_i in each iteration. We set the revised estimate P_i^{r+1} to be

$$P_i^{r+1}=\beta P_i^r(1-\beta)\left[\varepsilon\tilde{P}_i^{r+1}+\frac{(1-\varepsilon)}{2}(\tilde{P}_{i-1}^{r+1}+\tilde{P}_{i+1}^{r+1})\right], \tag{11b}$$

and we set $\beta=0.6$, $\varepsilon=0.5$ in all of the applications presented in this paper. The solutions discussed below are not at all sensitive to the values of β and ε.

Lucy's method was designed for positive kernels, which in his paper are interpreted as probability distributions. For our applications, the kernel has negative regions, as shown in Fig. 2. The negative tails in $g(k\varpi)$ can cause the $\tilde{P}_i$ to change sign (equation 11a). This is clearly undesirable, because $P(k)$ must be everywhere a positive function of k. This problem is especially acute if the true underlying power spectrum decreases steeply at long wavelengths. A poor initial guess for $P(k)$ in such cases can lead to negative power spectra at the first iteration. This problem is easily solved: if $\tilde{P}_i^{r+1}$ is negative, then we ignore the second term in (11b) and set $\beta=0.2$ (again the results are insensitive to β). As described in the next section, with these modifications we find that Lucy's algorithm provides reliable and stable inversions to realistic test problems. Any remaining instabilities in the inversion are usually caused by the use of too narrow a range of k and ϖ. These instabilities are always easily identified, since the angular correlations $w(\varpi)$ computed from equation (10) provide a poor match to the observed correlation function.

4.2 Tests of the method

We first test how well the method can recover a known form of the power spectrum:

$$P(k)\propto\frac{k}{k_c^2+k^2}. \tag{12}$$

We calculate the angular correlation function by integrating equation (5a) numerically using the kernel of Fig. 2. The resulting angular correlation functions are plotted as the solid lines in Figs 3(b) and (d) for the cases $k_c=0.01$ and 0.1 h Mpc^{-1}. The analytic power spectra are shown as the solid lines in Figs 3(a) and (c). For the initial guess, we set $P_i k^2\propto k^{0.8}$ as appropriate for a power-law correlation function $\xi(r)\propto r^{-1.8}$, and adjusted the initial power spectrum to reproduce roughly the amplitude of $w^o(\varpi)$. The initial guesses and each alternate iteration are plotted in Fig. 3, up to a maximum of 10 iterations. In the example shown in Figs 3(a) and (b), the solution converges quickly to the correct answer. The solution is remarkably stable, and we can continue for over a hundred iterations with imperceptible changes from the final solution plotted in the figure.

The example shown in Figs 3(c) and (d) is more difficult than the previous example, because the correlation function changes sign at $\varpi\sim0.04$ and has a minimum of $\sim-2\times10^{-3}$ at $\varpi\sim0.08$. After 10 iterations, we find an excellent approximation to the true power spectrum over the entire range of wavenumbers plotted in the figure, and we succeed in recovering a reasonable approximation to the negative peak in $w(\theta)$. In this case, however, further iterations can lead to instabilities in $P(k)$ (depending on the ranges of k and ϖ), and it proves difficult to improve much on the final estimate plotted in Fig. 3. Fortunately, it is always easy to detect an instability, because the estimates of the angular correlation function w_i^r computed from P_i^r begin to diverge from the correct answer w^o. In our tests we have found that instabilities are almost always associated with angular correlation functions that have negative tails. The inversions of angular correlation functions that are everywhere positive are usually extremely stable.

In the next example, we show how an angular correlation function with a smooth and apparently innocuous form,

$$w(\varpi)\propto\frac{\varpi^{-0.8}}{[1+(\varpi/\varpi_0)^4]}, \qquad \varpi_0=0.05, \tag{13}$$

can result from a power spectrum that contains a bump. Equation (13) is plotted as the solid line in Fig. 4(b), and the initial guess for $P_i k^2$ is plotted as the solid line in Fig. 4(a). Each alternate iteration is plotted as a dotted line in Fig. 4, and we see that the method converges quickly to a power spectrum that contains a bump at $k\sim0.1$ h Mpc, rising above the asymptotic form $P_i k^2\propto k^{0.8}$ and then falling steeply at lower wavenumbers. The existence of such a long-wavelength feature in the power spectrum could offer an important test for theories of structure formation, but a bump in the power spectrum could easily escape detection in $w(\theta)$ unless one had some prior expectation of its presence. The tests shown in Figs 3 and 4 demonstrate that the bump in the power spectrum in Fig. 4 is clearly a result of the shape of $w(\theta)$, and is not caused by errors in the inversion.

5 APPLICATION TO THE APM GALAXY SURVEY

Fig. 5 shows $w(\theta)$ measured from the APM Galaxy Survey for galaxies in the magnitude range $17\leq b_J\leq20$. These estimates are identical to those plotted in fig. 1 of M90, and are the average of $w(\theta)$ measured from four zones of the

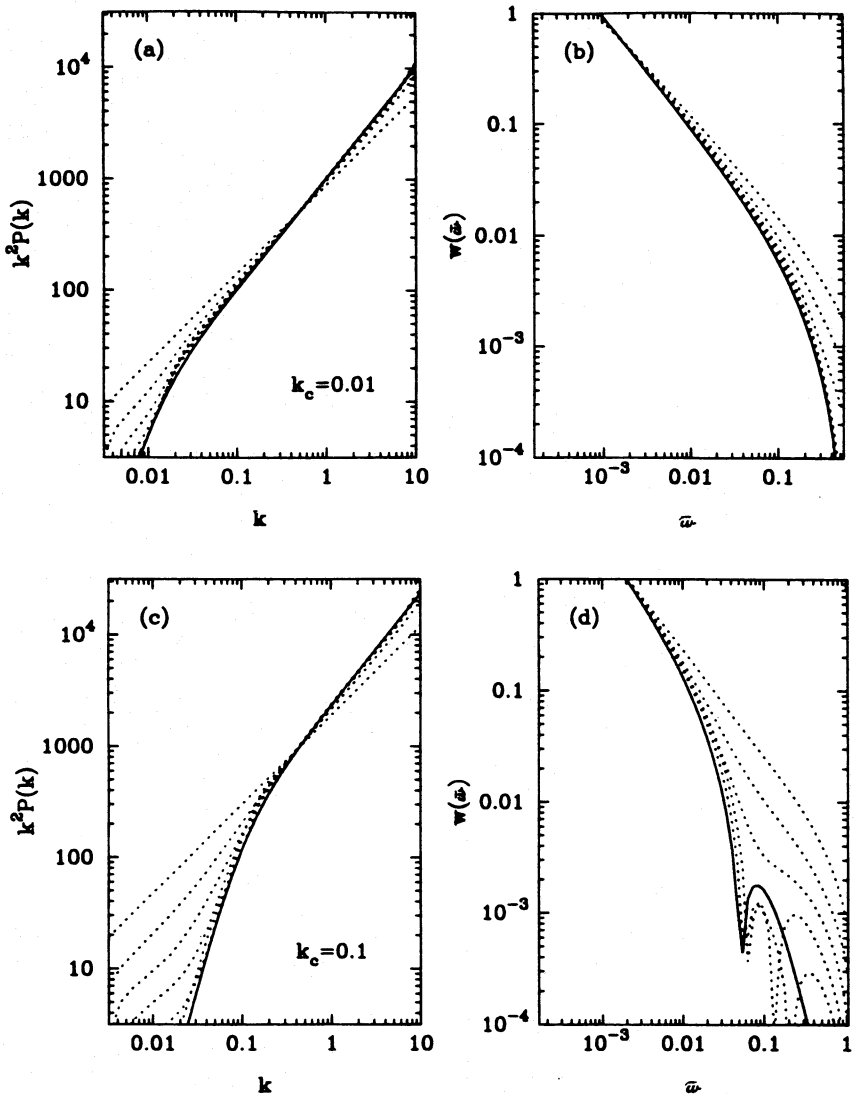

Figure 3. Figures illustrating how Lucy's method converges to a solution of the integral equation. In these tests we specify the functional form of the power spectra, shown as the solid lines in (a) and (c). The angular correlation functions derived from these power spectra are shown by the solid lines in (b) and (d). The dotted lines show the power-law initial guess for the power spectrum, and each alternate iteration until the final one after 10 iterations. The dotted lines in (b) and (d) show the angular correlation functions computed from the sum (10) from the power spectra shown in (a) and (c). (a) and (b) are for the power spectrum of equation (12) with $k_c = 0.01\ h$ Mpc^{-1}, and (c) and (d) are for $k_c = 0.1\ h$ Mpc^{-1}. The units of k are h Mpc^{-1}.

APM survey of roughly equal area. The error bars plotted in Fig. 5 show $\pm 2\sigma$ errors computed from the scatter of the estimates for the four zones. The inset in Fig. 1 of M90 shows that $w(\theta)$ is consistent with zero on scales $\theta \gtrsim 7°$. On these angular scales, the errors in $w(\theta)$ are probably dominated by systematic errors in the catalogue, which we have estimated can introduce offsets of $\sim 1 \times 10^{-3}$ in $w(\theta)$ on the scale of a single plate (Maddox et al. 1990b). The effects of systematic errors on $P(k)$ are discussed in more detail below.

Although these data points define a reasonably smooth function, we have fitted them to a parametric form for $w(\theta)$. This ensures that the inverted power spectrum is smooth. We compare this inversion with the results of inverting a linear interpolation through the data points below. The parametric form that we have adopted,

$$w(\varpi) = A(\varpi')^{-\beta} \exp\left[-2\left(\frac{\varpi'}{\varpi_0'}\right)^2\right] + \frac{B(\varpi')^{-\beta_2}}{[1+(\varpi'/\varpi_1')^{\beta_1}]},$$

$$\varpi' = 180\varpi/\pi, \qquad (14)$$

is quite flexible, and contains seven free parameters which we fit to the data by least-squares minimization.

The parameters determined from fits to the data points in Fig. 5 are given in the first row of Table 1; the fit is plotted as the solid curve in the figure. Parameters for fits to the tops and bottoms of the 2σ error bars plotted in Fig. 5 are given in the second and third rows in the table; the corresponding fits are shown as the dotted curves in the figure. The fit to the mean of the data points provides a very accurate description of the APM data points. The fits to the tops and bottoms of

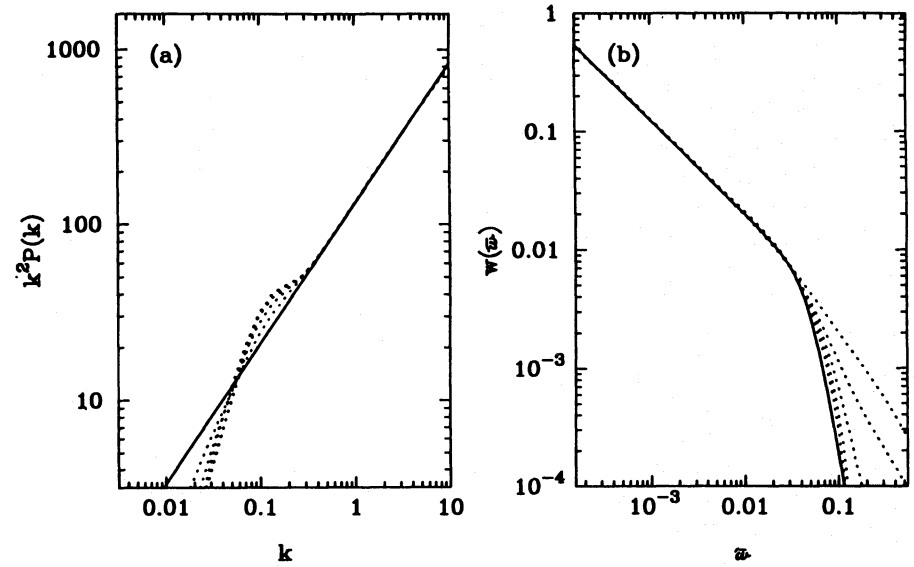

Figure 4. As Fig. 3, except here we have specified the form of $w(\varpi)$ (equation 13). After 10 iterations, the power spectrum converges to a form that has a feature at $k_c \sim 0.1\ h\ \mathrm{Mpc}^{-1}$, rising above the power law appropriate on small scales.

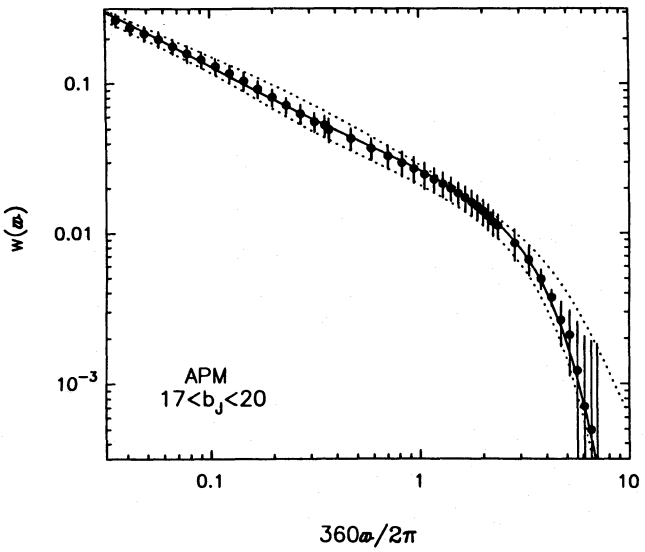

Figure 5. The points show the angular correlation function of the APM Galaxy Survey for the magnitude range $17 \le b_J \le 20$ (from fig. 1 of Maddox et al. 1990a). The error bars show 2σ errors computed from the scatter in $w(\varpi)$ measured in four zones of the APM survey of roughly equal area. The solid and dotted lines show least-squares fits of the parametric form equation (14) to the points, the tops and bottoms of the error bars.

the error bars are not as accurate, but they provide a reasonable indication of the random errors in $w(\varpi')$. The fits to equation (14) give positive values of $w(\varpi')$ at all angles, though in fact the data points cross zero at angles $\theta \sim 7°$ and have an average value of approximately -5×10^{-4} over the range 7° to 20° (see fig. 1 of M90). However, as noted above, the systematic errors in the APM data are expected to be larger than this, and to dominate the errors at values of $w \lesssim 10^{-3}$. The fitting function has been chosen to provide an accurate description of the APM angular correlations over the range where $w(\theta)$ exceeds 10^{-3}.

The main source of systematic errors in the APM survey is probably the large-scale gradients in the galaxy density arising from inaccuracies in matching the $6° \times 6°$ photographic plates to form the mosaic of 180 plates. These systematic errors have been discussed at length by Maddox et al. (1990c), who show that they introduce offsets of $\lesssim 1\text{–}2 \times 10^{-3}$ on the scale of a single plate (see section 2 and figs 14 and 16 of Maddox et al. 1990b). This analysis is confirmed by a comparison of APM magnitudes with CCD photometry of over 12 000 galaxies taken by Tucker et al. (1992) as part of the Las Campanas Deep Redshift Survey. An analysis of these CCD magnitudes by Maddox et al. (1993, in preparation) shows that the systematic errors in $w(\theta)$ are $\lesssim 2 \times 10^{-3}$ on a scale of a few deg, and may well be half this value.

Table 1. Parameters of fits to APM $w(\varpi)$.

	A	β	ϖ_0'	B	ϖ_1'	β_1	β_2
$w(\varpi)$ mean	0.0281	0.575	5.27	0.0197	0.0725	1.56	0.527
$w(\varpi)$ $+2\sigma$ errors	0.0212	0.720	7.62	0.0352	0.364	1.17	0.151
$w(\varpi)$ -2σ errors	0.0226	0.598	5.30	0.0066	0.174	2.50	0.743

To illustrate the possible effects of artificial gradients in the APM survey caused by plate-matching errors, we subtract the following function from the points in Fig. 5:

$$w_{\rm err}(\varpi) = \frac{2\times10^{-3}}{[1+(\varpi'/6)^2]}. \qquad (15)$$

This function subtracts 2×10^{-3} from $w(\theta)$ over most of the range shown in Fig. 5, and 1×10^{-3} on the plate scale of $\sim 6°$ as in the model for large-scale gradients described by Maddox et al. (1990b). The function (15) was chosen so that the offset declines to zero smoothly as $\varpi \to \infty$; this function is preferable to an approximation of the systematic errors by a constant offset, giving better stability in the numerical inversion of the power spectrum.

Fig. 6 shows the equivalent of the test shown in Fig. 4, but applied to the best fit to the APM data points (solid curve in Fig. 5). We start with an initial guess $P(k) \propto k^{-1.2}$, and within a few iterations the solution reaches the form shown in which the power spectrum has a bump at $k \sim 0.1\ h\ \mathrm{Mpc}^{-1}$, similar to the example shown in Fig. 4. As Fig. 6 shows, the inversions are stable and converge rapidly.

The power spectrum of Fig. 6 is plotted as the thick solid line in Fig. 7. The inversions of the fits to the tops and bottoms of the APM error bars are plotted as the dotted lines. The dashed line shows the inversion of the fit to the APM data points from which we have subtracted equation (15) to model the systematic errors. Evidently, the APM survey provides an accurate estimate of the three-dimensional power spectrum for wavenumbers $\gtrsim 0.05\ h\ \mathrm{Mpc}^{-1}$. On small scales, the power spectrum is a power law with a slope $P(k) \propto k^{-1.25}$, but the inversion rises above this power law on scales $k \lesssim 0.2\ h\ \mathrm{Mpc}^{-1}$, and flattens off at wavenumbers $k \sim 0.08\ h\ \mathrm{Mpc}^{-1}$. Notice that there is no firm evidence for a turnover in the APM power spectrum at long wavelengths.

Fig. 8 shows a check of the inversions. In this figure, we plot numerical integrations of $w(\varpi)$, using the power spectra plotted in Fig. 7. These give curves that are almost indistinguishable from the fits to $w(\varpi)$ shown in Fig. 5. The dashed line crosses zero at $\theta \approx 6°$, as expected from equation (15). Clearly the power spectra plotted in Fig. 7 are the correct inversions of the APM angular correlation functions.

Another indication of the errors in $P(k)$ can be obtained by inverting linear interpolations of the APM angular correlations measured for each of the four zones, with no

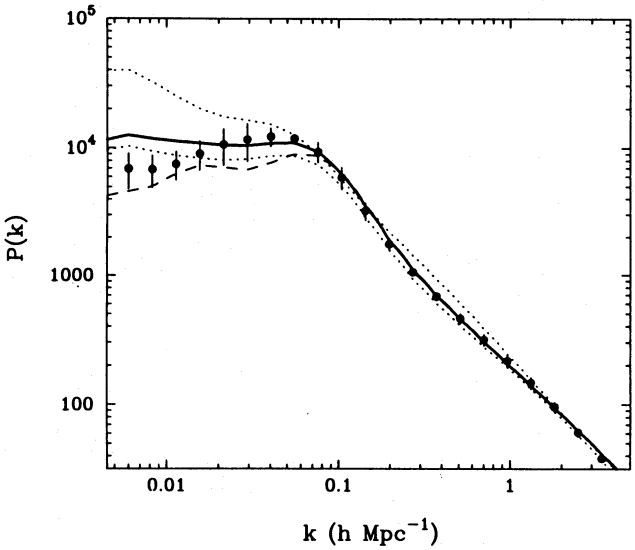

Figure 7. Three-dimensional power spectra inverted from $w(\varpi)$ measured from the APM survey using the kernel shown in Fig. 1. The solid and dotted lines show the inversions of the fits to $w(\varpi)$ shown as the solid and dotted lines in Fig. 4. The dashed line shows how a systematic error in the APM $w(\varpi)$, modelled by equation (15), affects the three-dimensional power spectrum. The points show the average of the estimates of $P(k)$ from linear interpolations of the $w(\theta)$ data points from the four zones together with 1σ error bars (see Fig. 9).

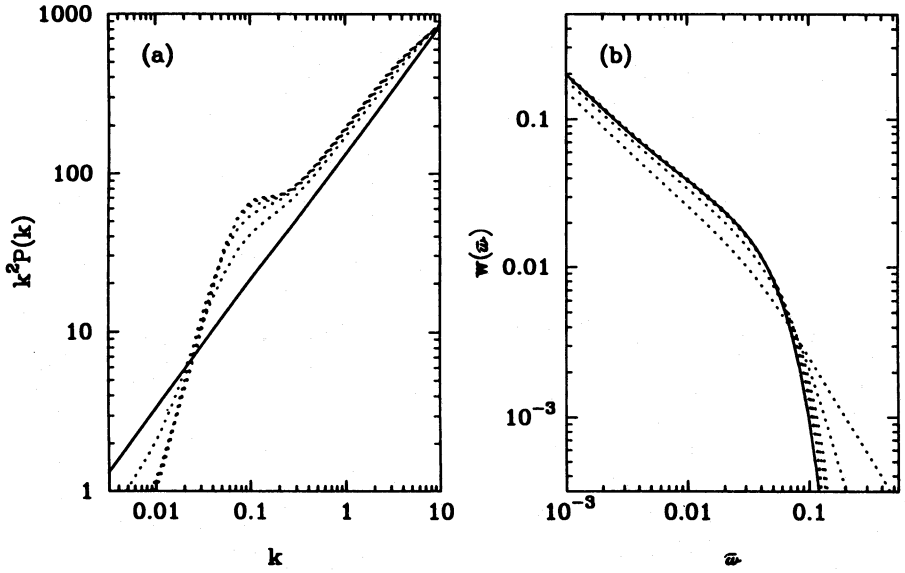

Figure 6. Convergence of Lucy's method for the power spectrum of the APM Galaxy Survey (as Figs 3 and 4). In this plot we show the inversion of the best-fitting $w(\varpi)$ to the APM data points (solid line in Fig. 5).

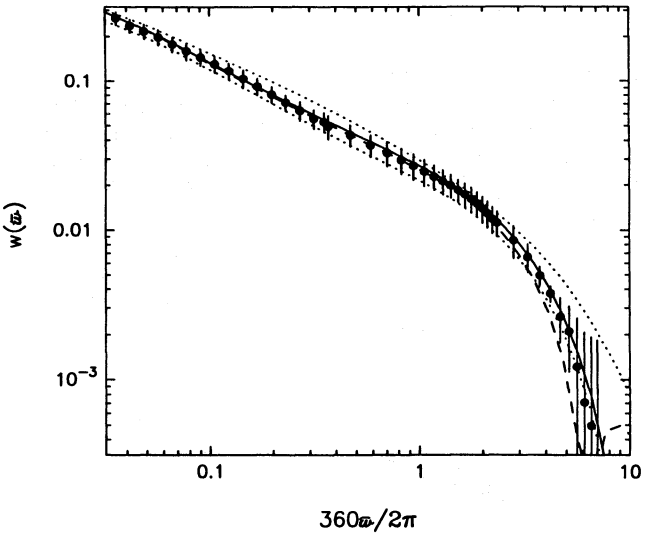

Figure 8. Angular correlation functions computed from the curves shown in Fig. 7 compared with the APM data illustrating the accuracy of the inversion.

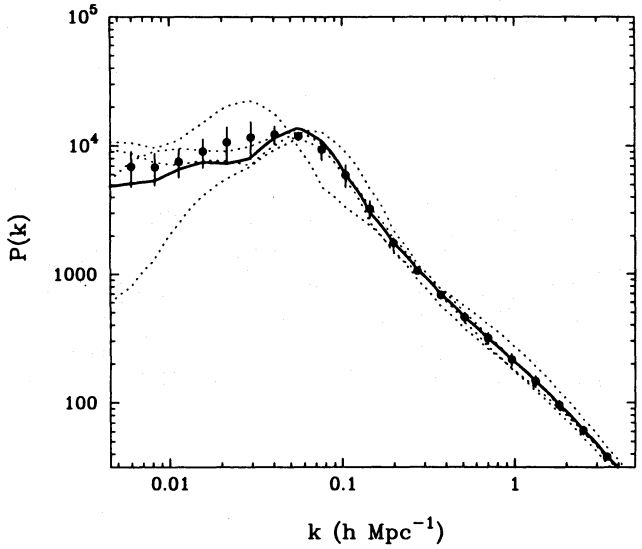

Figure 9. Three-dimensional power spectra inverted from $w(\varpi)$ computed from linear interpolations of the $w(\theta)$ data points. The dotted lines show $P(k)$ determined from each of the four zones. The thick solid line shows $P(k)$ determined from the average of $w(\theta)$ over the four zones. The points show the average of the estimates of $P(k)$ from the four zones together with 1σ error bars.

smoothing of the data or constraints that force the correlation function to be positive on large angular scales. These inversions are shown by the dotted lines in Fig. 9. It is interesting that three zones give similar power spectra which peak at wavenumbers $\sim 0.06\ h$ Mpc^{-1}, while $P(k)$ for the fourth continues to rise until $k \sim 0.02\ h$ Mpc^{-1}. Even in a sample as large as the APM Galaxy Survey, the random errors on $w(\theta)$ lead to large errors in the power spectrum at small wavenumbers. The points show the average of the four dotted lines and the 1σ dispersion. These points are also plotted in Fig. 7. The thick solid line in Fig. 9 shows the

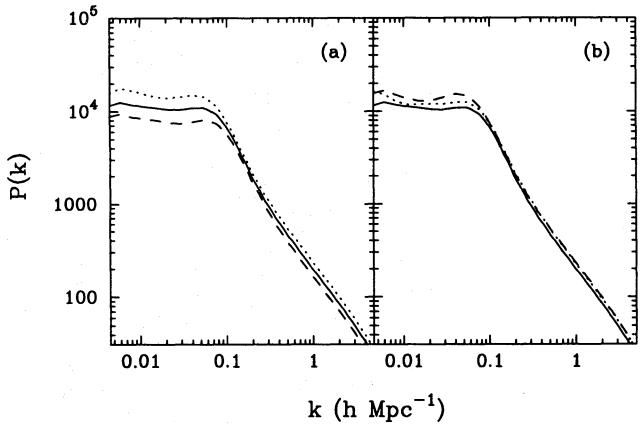

Figure 10. Sensitivity of the inversion to errors in the redshift distribution evolution and cosmological model. The solid lines in (a) and (b) are identical to the solid line in Fig. 7 (i.e. $\alpha = 0$, $\Omega = 1$). The dotted and dashed lines in (a) show the result of increasing and decreasing the median redshift of the APM survey by 12 per cent respectively, keeping all other parameters fixed. In (b), we use the redshift distribution given by equations (7) and (8), but vary the evolution and cosmological model. The dotted line shows $\alpha = 1.2$, $\Omega = 1$, and the dashed line shows $\alpha = 0$, $\Omega = 0$.

inversion of the linear interpolation of the average $w(\theta)$ for the four zones. The average $P(k)$ over the four zones is in excellent agreement with the inversion of the parametric form (14) fitted to the data points for all wavenumbers $\gtrsim 0.01\ h$ Mpc^{-1}. At smaller wavenumbers, however, it is clear that both the random and systematic errors become very large and the APM survey provides little useful information on $P(k)$.

Errors in the model for the redshift distribution of the APM survey will cause errors in the three-dimensional power spectrum. Uncertainties in the value of the median redshift cause a much larger change in the power spectrum than deviations of the shape of the redshift distribution from the form given in equation (7). From the Broadhurst et al. (1988) survey, the scatter in the median redshift over five fields has a standard deviation of 6 per cent. The median redshift at a magnitude limit of $b_j \sim 20$ given by equation (8a) is therefore extremely unlikely to be in error by more than 12 per cent, and so we adopt this as a generous estimate of the error in the redshift distribution. The solid line in Fig. 10(a) is identical to the solid line plotted in Fig. 7. The dotted and dashed lines show the effects of increasing and decreasing the median redshift by 12 per cent respectively. An error of this size leads to a change of about 20 per cent in the amplitude of $P(k)$, but leaves the shape almost unchanged. The range plotted in Fig. 10(a) is likely to overestimate the uncertainties arising from the errors in the redshift distribution.

Fig. 10(b) shows the sensitivity of the inversion to the evolution of the power spectrum and the cosmological model. We plot the solid line from Fig. 7, which was computed from the kernel plotted in Fig. 2, i.e. $\alpha = 0$ (the power spectrum is constant in comoving coordinates) and $\Omega = 1$. The dotted line shows the inversion for $\alpha = 1.2$ (i.e. a power spectrum of form $P(k) \propto k^{-1.2}$ is constant in physical coordinates) and $\Omega = 1$, and the dashed line shows $\alpha = 0$, $\Omega = 0$. In each case, the figures have similar shapes but are slightly offset from each other. At the depth of the APM survey,

evolutionary corrections and cosmology do not affect the shape of the power spectra very much. However, uncertainties in the evolution of $P(k)$ in deeper samples could limit the usefulness of the inversion technique.

6 DISCUSSION

Several authors have published three-dimensional power spectra for various galaxy redshift samples. In Fig. 11, we compare some of these with our inversion of $P(k)$. The filled circles show the convolved power spectrum $\tilde{P}(k)$ for the 1.2-Jy *IRAS* redshift survey (Fisher et al. 1993), the filled stars show Kaiser's (1991) estimates of $P(k)$ for the 0.6-Jy QDOT survey, and the open triangles show the results of Vogeley et al. (1992) for the CfA survey. In each case, we have plotted the power spectra measured in redshift space, which will differ from the power spectra in real space because of the distortions caused by peculiar velocities. Peacock & Nicholson (1991) have computed the power spectrum of a sample of radio galaxies, but this will not be discussed in detail here; the power spectrum of their sample has a similar shape to that of the CfA sample at wavenumbers $\lesssim 0.1\ h\ \mathrm{Mpc}^{-1}$ and has comparable errors (see fig. 1 of Vogeley et al. 1992), but with an amplitude that is three times higher.

The power spectra measured for the 1.2- and 0.6-Jy *IRAS* surveys should be almost the same, but in fact the QDOT results are systematically higher than the 1.2-Jy results at $k \lesssim 0.1\ h\ \mathrm{Mpc}^{-1}$ by about two standard deviations. The 1.2-Jy power spectrum has not been deconvolved to take into account the window function of their adopted survey geometry, but this should not affect the estimates by more than 15 per cent at the smallest wavenumbers plotted (see Fisher et al. 1993), which is much smaller than the differences in the *IRAS* power spectra plotted in Fig. 11. This discrepancy is disturbing and deserves further investigation. It may indicate that the errors in $P(k)$ have been underestimated, that there is a systematic difference between the two catalogues, or that the discrepancy is caused by differences in the estimation techniques.

The CfA power spectrum has large error bars at wavenumbers $\lesssim 0.08\ h\ \mathrm{Mpc}^{-1}$. At larger wavenumbers, the CfA power spectrum sits high in comparison to the power spectrum determined from the APM survey. This could perhaps be caused by peculiar velocities. According to linear perturbation theory, the power spectrum measured in redshift space will be higher than the power spectrum measured in real space by a factor

$$f = \left(1 + \frac{2}{3}\frac{\Omega_0^{0.6}}{b} + \frac{1}{5}\frac{\Omega_0^{1.2}}{b^2}\right) \tag{16}$$

(Kaiser 1987), where b is a 'biasing' factor relating fluctuations in the galaxy distribution to fluctuations in the mass, $(\delta\rho/\rho)_{\mathrm{gal}} = b(\delta\rho/\rho)_{\mathrm{mass}}$. However, the CfA points in Fig. 11 lie about a factor of 2 higher than the APM power spectrum, but this would imply $b/\Omega^{0.6} \lesssim 1$ from equation (16), which seems unreasonably low and disagrees with the lack of redshift-space distortion seen in the analysis of the Stromlo/APM redshift survey (Loveday et al. 1992b). We do not regard this discrepancy as particularly serious, because the errors in the CfA power spectrum are large. It is worth noting that the amplitudes of the APM power spectra plotted in Figs 7 and 10 seem quite reasonable when compared with

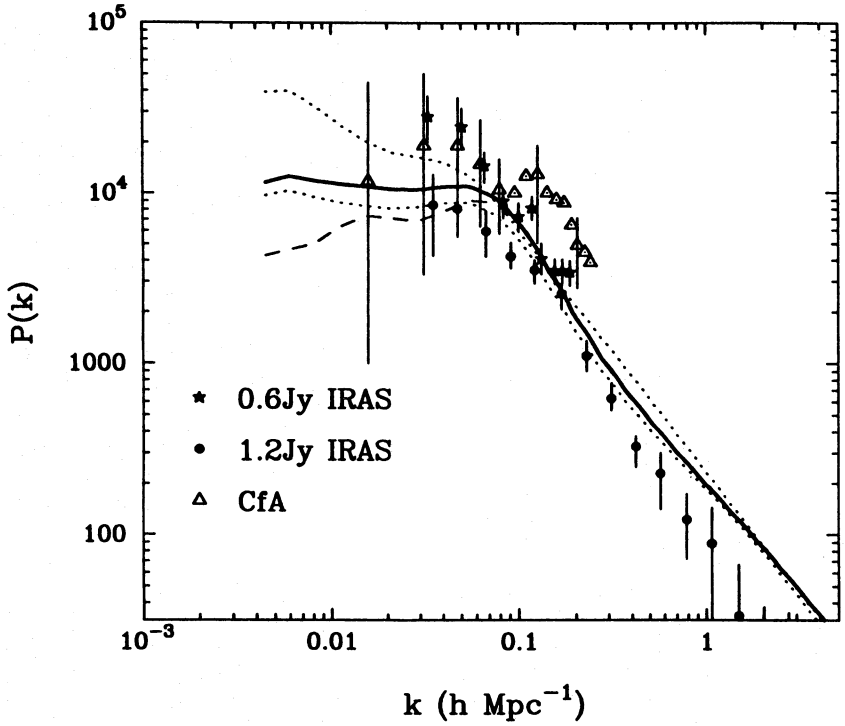

Figure 11. The power spectra for the APM Galaxy Survey from Fig. 7 plotted against redshift-space estimates of the power spectra from the QDOT 0.6-Jy *IRAS* survey (Kaiser 1991), the 1.2-Jy *IRAS* survey (Fisher et al. 1993) and the CfA redshift survey (Vogeley et al. 1992).

the amplitudes of the correlation functions measured from other surveys. Computing the variance of the fluctuations in spheres of radius $x_0 = 8\ h^{-1}$ Mpc,

$$\sigma^2_{x_0} = \frac{9}{2\pi^2}\int_0^\infty \frac{P(k)k^2}{(kx_0)^6}[\sin(kx_0) - kx_0\cos(kx_0)]^2\,\mathrm{d}k \qquad (17)$$

from the APM power spectra in Fig. 11, we find values of σ_8 in the range 0.76–0.88, with the best-fitting curve giving $\sigma_8 = 0.83$. These values are close to the value $\sigma_8 \sim 1$ determined from the 14.5-mag CfA survey (Davis & Peebles 1983). It is possible that our estimate of σ_8 is uncertain by ~ 20–30 per cent, because of uncertainties in the cosmological model and the evolution of $P(k)$, and errors in the redshift distribution of the APM survey (cf. Fig. 10).

In Fig. 12, we compare the APM power spectrum with the linear-theory power spectra of scale-invariant, adiabatic, cold dark matter (CDM) models. The two solid curves show power spectra for the 'standard' CDM model, i.e. with $\Gamma = \Omega h = 0.5$ and for $\Gamma = 0.2$ (equation 7 of Efstathiou, Bond & White 1992a, hereafter E92). In this figure, the APM power spectrum has been divided by a factor of 4 (i.e. the power spectrum matches the amplitude of the power spectrum of the mass fluctuations if $b_{\rm APM} = 2$), and the theoretical curves have been normalized at long wavelengths to match the amplitude of the anisotropies in the microwave background radiation detected by *COBE* (Smoot et al. 1992); in deriving this normalization, we have assumed that $\Omega_0 = 1$, and that temperature fluctuations from gravitational waves are negligible (equations 5 and 6 of E92). The region labelled

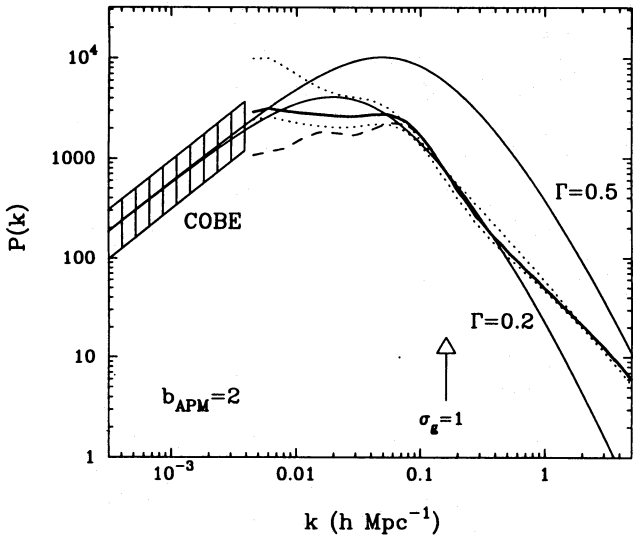

Figure 12. The power spectra of Fig. 5 divided by a factor of 4 (i.e. $b_{\rm APM} = 2$) compared to the linear power spectra of two CDM models with $\Gamma = 0.5$ ('standard' CDM) and $\Gamma = 0.2$ normalized to match the *COBE* temperature fluctuations on large scales assuming $\Omega = 1$. The hatched area shows the range of amplitudes allowed by the *COBE* observations for scale-invariant, adiabatic fluctuations if scalar perturbations dominate (i.e. temperature fluctuations created by gravitational waves are negligible). The arrow shows roughly the wavenumber at which fluctuations in the galaxy distribution have a variance of unity [$\sigma(x_0) = 1$, plotted at wavenumber $k_0 = 1/x_0$ computed from equation (17) for the power spectrum plotted as the thick solid line].

COBE shows the range of amplitudes allowed by the *COBE* measurements for a scale-invariant, adiabatic spectrum; the upper limit $k \sim 0.003\ \Omega_0^{0.41}\ h$ Mpc^{-1} of this region is set by the 7° resolution of the *COBE* DMR experiment.

The $\Gamma = 0.5$ curve cannot be adjusted to fit the shape of the APM power spectrum for any value of $b_{\rm APM}$ (see M90). The $\Gamma = 0.2$ curve provides a much better match to the APM power spectrum up to wavenumbers $k \sim 0.3\ h$ Mpc^{-1}, and, as we have noted elsewhere, it provides a good phenomenological match to the angular correlation function of the APM Galaxy Survey and to the spatial correlation function of rich APM clusters (Efstathiou et al. 1990b, 1992b; Efstathiou 1993). We would not expect the linear power spectrum to match the observations at larger wavenumbers, since the mass fluctuations are non-linear on these scales. The arrow plotted in Fig. 12 shows the wavenumber $k_0 = 1/s_0$ at which fluctuations in the galaxy distribution have unit variance, computed from equation (17) for the APM power spectrum plotted as the thick line in the figure.

The most plausible way to realize the $\Gamma = 0.2$ curve would be to add a cosmological constant to a low-density CDM universe, so that the geometry is spatially flat as predicted by the inflationary model (e.g. Peebles 1984). In this case, a match to the *COBE* microwave background anisotropies requires lower values of $b_{\rm APM}$, in the range ~ 0.8–1.3, depending on the value of h (see E92, fig. 2; see also Kofman, Gnedin & Bahcall 1993). As noted by several authors (e.g. Davis, Summers & Schlegel 1992; Taylor & Rowan-Robinson 1992, and references therein), it is unclear whether amplitudes in this range are compatible with observed streaming motions in a low-density universe. Although the $\Gamma = 0.2$ curve provides a rough match to the APM power spectrum at long wavelengths, it fails to fit the 'bump' accurately in the APM power spectrum at $k \approx 0.2\ h$ Mpc^{-1}. This slight discrepancy is noticeable also in fig. 1 of E92, where the $w(\theta)$ curve for a $\Gamma = 0.2$ model lies below the APM measurements on angular scales $2° \lesssim \theta \lesssim 6°$.

Recently, there has been renewed interest in the possibility that the excess power in the galaxy distribution arises from 'mixed' dark matter (MDM), i.e. that about 10–30 per cent of the critical density is contributed by massive neutrinos, and most of the rest is made up of cold dark matter with the remainder in baryons (see Davis et al. 1992; Taylor & Rowan-Robinson 1992; Schaefer & Shafi 1992; for earlier work see Shafi & Stecker 1984; Bardeen, Bond & Efstathiou 1987; Schaefer, Shafi & Stecker 1989; Holtzman 1989). Fig. 13 shows the linear power spectra for two MDM models from Holtzman (1989), normalized to the *COBE* amplitude on large scales. These models just about match the APM power spectra at k—0.1 if $b_{\rm APM} \sim 1.2$, but only if the systematic errors in the APM survey are as large as in equation (15). At larger wavenumbers, the APM power spectrum lies well above the theoretical spectrum for $\Omega_\nu = 0.3$. In contrast, Taylor & Rowan-Robinson (1992) argue that a linear MDM power spectrum with $\Omega_\nu = 0.3$ provides a good match to the power spectrum of *IRAS* galaxies over the wavenumber range $0.05 \lesssim k \lesssim 1\ h$ Mpc^{-1}. However, in making this comparison, they inferred the power spectrum and its errors from measurements of galaxy variances, rather than by estimating the power spectrum directly (cf. the estimates plotted in Fig. 11); moreover, in comparing the theoretical predictions with observations, they took no

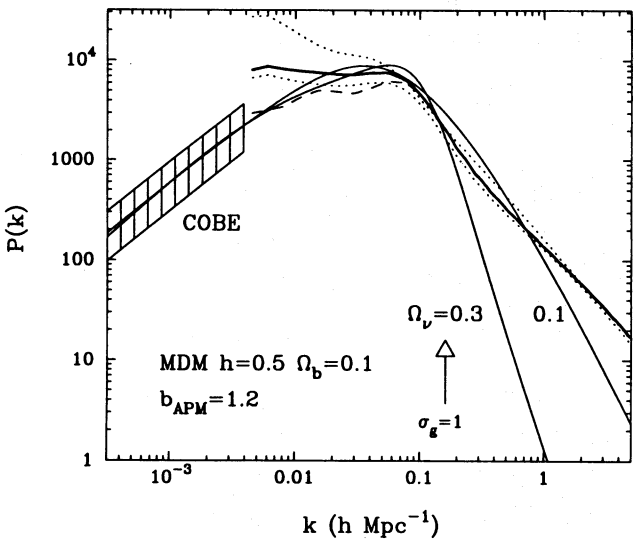

Figure 13. As Fig. 12, except that we have divided the APM power spectrum by a factor of 1.44 ($b_{APM}=1.2$). We have plotted linear power spectra for two MDM models from Holtzman (1989), normalized to match the *COBE* anisotropies. These models have scale-invarient initial spectra, $h=0.5$, $\Omega_{CDM}+\Omega_b+\Omega_\nu=1$. $\Omega_b=0.1$, and $\Omega_\nu=0.3$ and 0.1 (as indicated in the figure).

account of non-linear evolution, or of the distortion of the clustering in redshift space caused by small-scale peculiar motions and redshift errors. The agreement that they find with the MDM linear power spectrum, particularly at wavenumbers $k\gtrsim 0.1\ h\,\mathrm{Mpc}^{-1}$, is fortuitous.

It is easy to understand the differences between Figs 12 and 13. The power spectrum of the $\Omega_\nu=0.1$ model has a similar shape to the 'standard' CDM model and hence requires a low bias, $b_{APM}\sim 1$, to match the long-wavelength region of the APM power spectrum and the *COBE* anisotropy measurements. However, for a low value of Ω_ν the amplitude of the power spectrum on small scales is high; for example, the power spectrum with $\Omega_\nu=0.1$ plotted in Fig. 13 gives $\sigma_8=0.83$ for the amplitude of the mass fluctuations. This is significantly larger than the values of $\sigma_8\sim 0.5$–0.6 inferred from the abundances of rich clusters of galaxies (White, Efstathiou & Frenk 1993). The curve with $\Omega_\nu=0.3$ plotted in Fig. 13 gives a more acceptable value $\sigma_8=0.59$, but it remains to be seen whether this model can match the small-scale clustering seen in the galaxy distribution. First results from numerical simulations by Klypin et al. (1993) indicate that it may be possible to match the observed non-linear correlations of galaxies, but their prescriptions for identifying galaxies in dissipationless models are schematic; more complex calculations, incorporating hydrodynamics, are required to address this point in detail.

There are many other possible models that we could compare with our results, for example, baryon isocurvature models (Peebles 1987a) and tilted CDM models (Cen et al. 1992), but we leave such comparisons to the interested reader. However, we mention here that it is worth investigating whether the feature at $k\sim 0.1\ h\ \mathrm{Mpc}^{-1}$ in the APM power spectrum could be identified with the matter–radiation Jeans mass in baryon isocurvature models (see the features in the power spectra plotted by Peebles 1987b and Efstathiou & Bond 1987, and the discussion by Jørgensen et al. 1993). It is also possible that this feature is associated with the 'periodicity' on scales of $\sim 120\ h^{-1}$ Mpc reported in pencil-beam redshift surveys (Broadhurst et al. 1990).

Our main goal has been to illustrate the technique for recovering the three-dimensional power spectrum from measurements of the angular correlation function, and to apply it to the APM survey. We find that the APM power spectrum is a power law at high wavenumbers, with slope $P(k)\propto k^{-1.25}$. At wavenumbers $k\sim 0.2\ h\ \mathrm{Mpc}^{-1}$, the power spectrum rises above the power law and then flattens at $k\lesssim 0.08\ h\ \mathrm{Mpc}^{-1}$, and perhaps declines at smaller wavenumbers. The shape of the APM power spectrum at large scales is matched approximately by a low-density CDM power spectrum with $\Gamma=0.2$. Mixed dark matter models can be adjusted to match the APM power spectrum at wavenumbers $k\lesssim 0.1\ h\ \mathrm{Mpc}^{-1}$ and to the *COBE* anisotropies on scales $k\lesssim 0.003\ h\ \mathrm{Mpc}^{-1}$. It is important to investigate the non-linear clustering of these models in detail to see whether they can match the APM power spectrum on scales $k\gtrsim 0.1\ h\ \mathrm{Mpc}^{-1}$.

ACKNOWLEDGMENTS

This work has been supported by the UK Science and Engineering Research Council. CMB acknowledges the receipt of an SERC research studentship. We thank Dr Cedric Lacey for comments on an earlier manuscript, and Dr S. J. Maddox for his many years of effort on the APM Galaxy Survey. We also thank Dr Karl Fisher for a very useful referee's report.

REFERENCES

Bardeen J. M., Bond J. R., Efstathiou G., 1987, ApJ, 321, 28
Baugh C. M., Efstathiou G., 1993, MNRAS, submitted
Broadhurst T. J., Ellis R. S., Shanks T., 1988, MNRAS, 235, 827
Broadhurst T. J., Ellis R. S., Koo D. C., Szalay A. S., 1990, Nat, 343, 726
Cen R., Gnedin N. Y., Kofman L. A., Ostriker J. P., 1992, ApJ, 399, L11
Colless M. M., Ellis R. S., Taylor K., Hook R. N., 1990, MNRAS, 244, 408
Colless M. M., Ellis R. S., Broadhurst T. J., Taylor K., Peterson B. A., 1993, MNRAS, 261, 19
Cowie L. L., Songaila A., Hu E. M., 1991, Nat, 354, 460
Davis M., Peebles P. J. E., 1983, ApJ, 267, 465
Davis M., Summers F. J., Schlegel D., 1992, Nat, 359, 393
Efstathiou G., 1993, in Proceedings of the US National Academy of Sciences, 90, 4859
Efstathiou G., Bond J. R., 1987, MNRAS, 227, 33P
Efstathiou G., Kaiser N., Saunders W., Lawrence A., Rowan-Robinson M., Ellis R. S., Frenk C. S., 1990, MNRAS, 247, 10P
Efstathiou G., Sutherland W. J., Maddox S. J., 1990b, Nat, 348, 705
Efstathiou G., Bernstein G., Katz N., Tyson J. A., Guhathakurta P., 1991, ApJ, 380, L47
Efstathiou G., Bond J. R., White S. D. M., 1992a, MNRAS, 258, 1P (E92)
Efstathiou G., Dalton G. B., Sutherland W. J., Maddox S. J., 1992b, MNRAS, 257, 125
Fall S. M., Tremaine S., 1977, ApJ, 216, 682
Fisher K. B., Davis M., Strauss M. A., Yahil A., Huchra J. P., 1993, ApJ, 402, 42
Groth E. J., Peebles P. J. E., 1977, ApJ, 217, 592
Holtzman J. A., 1989, ApJS, 71, 1
Jørgensen H. E., Kotok E., Naselsky P., Novikov I., 1993, preprint
Kaiser N., 1987, MNRAS, 227, 1

Kaiser N., 1991, in Holt S. S., Bennett C. L., Trimble V., eds, AIP Conf. Proc. 212, After the First Three Minutes. American Institute of Physics, New York, p. 248
Klypin A., Holtzman J., Primack J., Regos E., 1993, ApJ, submitted
Kofman L. A., Gnedin N. Y., Bahcall N. A., 1993, ApJ, 413, 1
Limber D. N., 1954, ApJ, 119, 655
Loveday J., Peterson B. A., Efstathiou G., Maddox S. J., 1992a, ApJ, 390, 338
Loveday J., Efstathiou G., Peterson B. A., Maddox S. J., 1992b, ApJ, 400, L43
Lucy L. B., 1974, AJ, 79, 745
Maddox S. J., Efstathiou G., Sutherland W. J., Loveday J., 1990a, MNRAS, 242, 43P (M90)
Maddox S. J., Efstathiou G., Sutherland W. J., 1990b, MNRAS, 246, 433
Maddox S. J., Sutherland W. J., Efstathiou G., Loveday J., Peterson B. A., 1990c, MNRAS, 247, 1P
Parry W. E., 1977, Phys. Lett., 60A, 265
Peacock J. A., 1991, MNRAS, 253, 1P
Peacock J. A., Nicholson D., 1991, MNRAS, 253, 307
Peebles P. J. E., 1980, The Large-Scale Structure of the Universe. Princeton Univ. Press, Princeton, Section 51
Peebles P. J. E., 1984, ApJ, 284, 439
Peebles P. J. E., 1987a, ApJ, 315, L51
Peebles P. J. E., 1987b, Nat, 327, 210
Phillipps S., Fong R., Ellis R. S., Fall S. M., MacGillivray H. T., 1978, MNRAS, 182, 673
Saunders W. et al., 1991, Nat, 349, 32
Schaefer R. K., Shafi Q., 1992, Nat, 359, 199
Schaefer R. K., Shafi Q., Stecker F. W., 1989, ApJ, 347, 575
Shafi Q., Stecker F. W., 1984, Phys. Rev. Lett., 53, 1292
Smoot G. et al., 1992, ApJ, 396, L1
Taylor A. N., Rowan-Robinson M., 1992, Nat, 359, 396
Tucker D. L., Oemler A., Shectman S. A., Lin H., Kirshner R. P., Schechter P. L., 1992, preprint
Vogeley M. S., Park C., Geller M. J., Huchra J. P., 1992, ApJ, 391, L5
White S. D. M., Efstathiou G., Frenk C. S., 1993, MNRAS, 262, 1023